Sensors and Actuators A 301 (2020) 111708

Contents lists available at ScienceDirect

Sensors and Actuators A: Physical

journal homepage: www.elsevier.com/locate/sna

Development of MMG sensors using PVDF piezoelectric electrospinning for lower limb rehabilitation exoskeleton

Cheng-Tang Pan[a,b,1], Chun-Chieh Chang[a], Yu-Sheng Yang[c,1], Chung-Kun Yen[a,*], Yu-Hsuan Kao[a], Yow-Ling Shiue[d,*]

[a] Department of Mechanical and Electro-Mechanical Engineering, National Sun Yat-sen University, Kaohsiung 80424, Taiwan
[b] Institute of Medical Science and Technology, National Sun Yat-sen University, Kaohsiung 80424, Taiwan
[c] Department of Occupational Therapy, Kaohsiung Medical University, Kaohsiung 80708, Taiwan
[d] Institute of Biomedical Sciences, National Sun Yat-sen University, Kaohsiung 80424, Taiwan

ARTICLE INFO

Article history:
Received 9 March 2019
Received in revised form 10 October 2019
Accepted 28 October 2019
Available online 3 November 2019

Keywords:
Mechanomyography (MMG)
Electromyography (EMG)
Lower limb rehabilitation exoskeleton (LLRE)
Piezoelectric
Polyvinylidene difluoride (PVDF)
Near-field electrospinning technology

ABSTRACT

In this study, a new type of fiber-based mechanomyography (MMG) sensor was developed and used as a motion on/off trigger sensor for a lower limb rehabilitation exoskeleton (LLRE). Piezoelectric material, polyvinylidene difluoride (PVDF), was applied to fabricate a MMG sensor, using the near-field electrospinning technology to electrically spin PVDF fibers to ~5-10 μm in diameter. PVDF fibers attached on an interdigitated (IDT) electrode with different pole pairs and interspaces were packaged into a MMG sensor. This MMG sensor was stuck on the thigh muscles to detect and acquire human motion intention signal, then trigger the controller and actuate the LLRE. The LLRE multi-axis control system included a master and four slave controllers. The master controller released the command signal to control the slave controllers via controller area network (CAN). A multi-axis control system was developed to actuate the joints of hips and knees of both legs by the LLRE. In the study, commercial electromyography (EMG) sensors were also to compare with the as-made MMG sensors. Results showed that the maximum signal amplitude of the commercail EMG sensor was about ~0.2 V, whereas the MMG sensor was about ~2.8 V. The signal-to-noise ratio (SNR) of EMG was about ~4, while that of MMG was about ~25. From physiological signals captured from the MMG sensor for the human walking with the LLRE, this new sensor improved the sensitivity in driving the LLRE.

© 2019 Elsevier B.V. All rights reserved.

1. Introduction

The pace of population ageing around the world is increasing dramatically. The dependence on medical aids may be gradually increased. Among those, the utilization of an exoskeleton will certainly gain more popularity as a medical human support in the near future. Exoskeletons comprise upper limbs [1], lower limbs [2,3] and whole body [4] exoskeletons. Using the lower limb exoskeletons could relieve inconvenience in moving lower limbs and helps the users to regain their self-esteem [5–7].

Nowadays, development of the trigger-driven sensors combined with physiological signals has become a new trend and the physiological signals are currently determined by the electromyography (EMG) sensors. The EMG sensor detects and records the electrical signals from the muscle's surface during motion and reflects its activity [8–10], which is very weak and minimal, unfortunately. During the measurement process, the signals can be easily interfered by external factors such as sweating or rough skin condition, leading to misjudgments. Therefore, studies on how to capture accurate muscle motion signals are intensive. In 1989, Orizio first proposed the mechanomyography (MMG) signal [11,12] with the advantage of signals were captured directly from the muscle vibration and was not affected by skin conditions [13]. Currently, most of the sensors are fabricated through the accelerometer and microphone processes [11–14], which were not sensitive enough to process complicated procedures. Moreover, the thin-film polymer polyvinylidene fluoride (PVDF) has been applied to MMG sensor for muscle detection. This included the hand muscles detection [15], skin softness detection [16], multifunctional pressure sensor [17] and gesture-recognition [18,19]. In above the case, the accuracy of the film type sensor judgment is insufficient for the complex deformation of the muscle.

* Corresponding authors.
E-mail addresses: alden0113@gmail.com (C.-K. Yen), shirley@imst.nsysu.edu.tw (Y.-L. Shiue).
[1] Contributed Equally.

https://doi.org/10.1016/j.sna.2019.111708
0924-4247/© 2019 Elsevier B.V. All rights reserved.

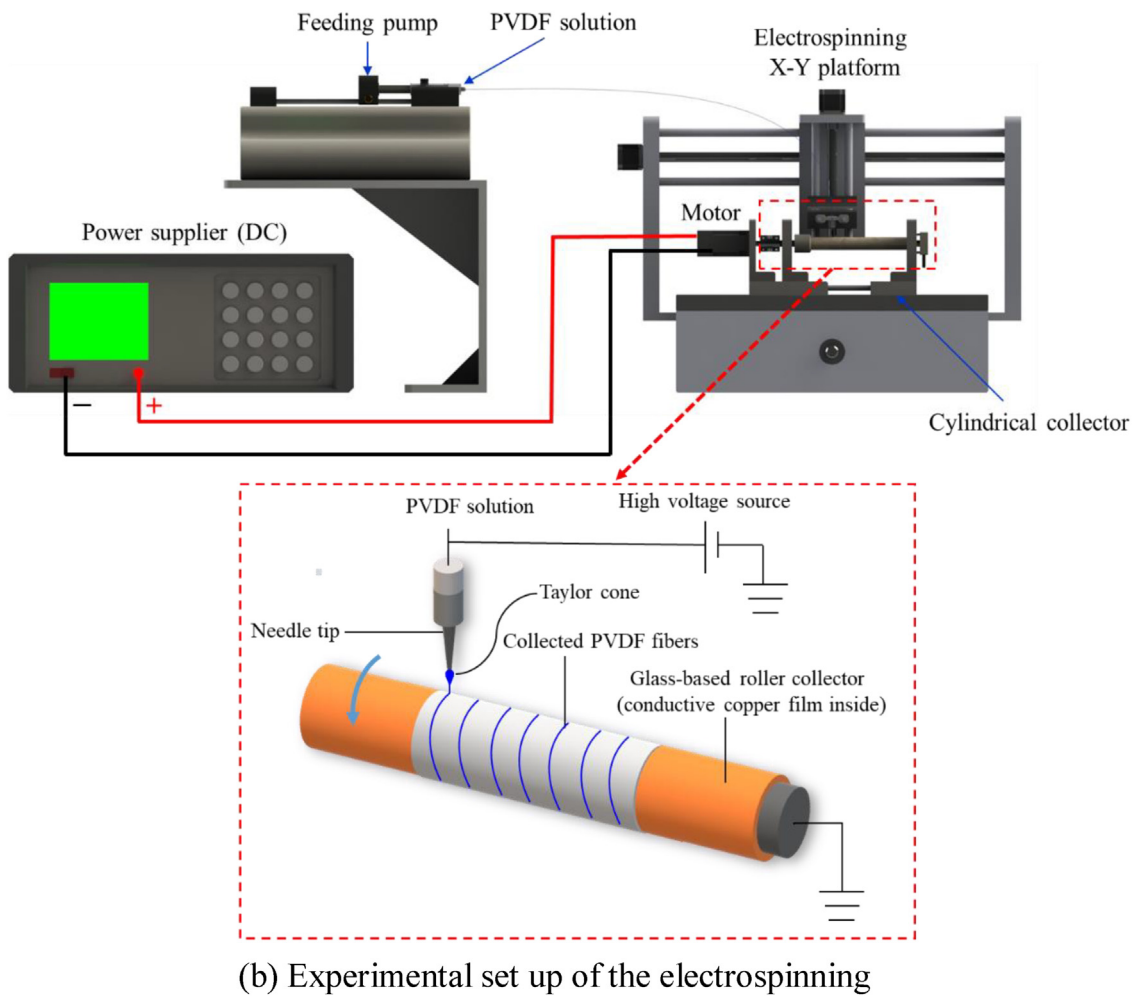

Fig. 1. Architecture of the electrospinning process. (b) Experimental set up of the electrospinning

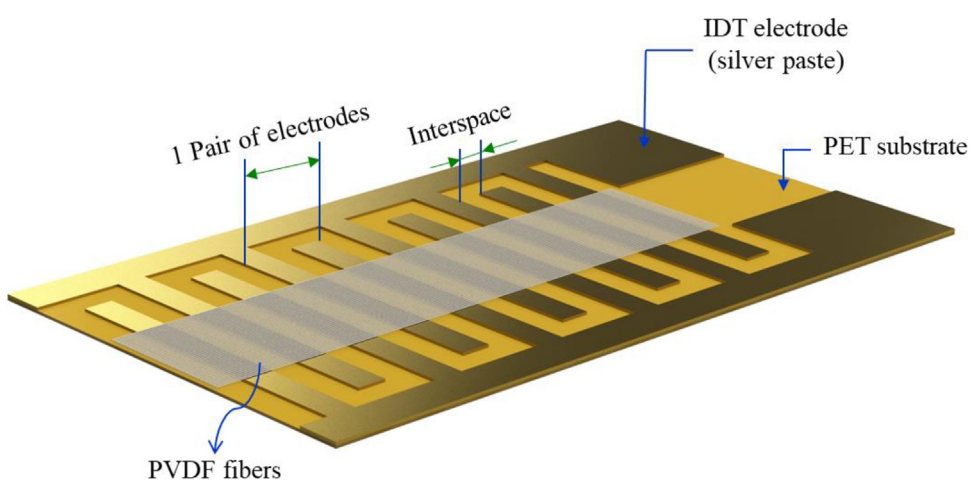

Fig. 2. Schematic diagram of the IDT electrode.

In this study, we developed a novel MMG sensor through the near-field electrospinning technology [20–23] and applied it to sense the human body motion for the lower limbs exoskeleton robot (LLRE). Using the MMG sensors, the signals were captured directly with high sensitivity from the muscle movement even when the body has a slight motion intention. The motion intention of the user can be accurately identified and to trigger the LLRE. Therefore, intention signals emerged from users with less mobility can be detected precisely using this sensitive MMG sensor.

In this study, we fabricated medical LLRE aids embedded with MMG sensors. The main goal was to develop a motor control technology and physiological signal sensor to capture physiological signals with high sensitivity. With this combination of the new

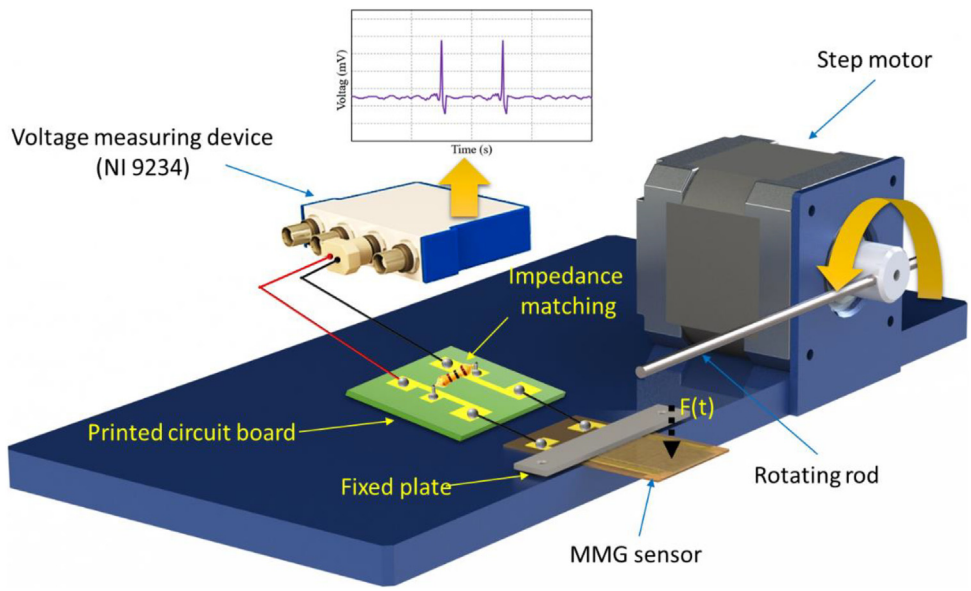

Fig. 3. Electrical measuring equipment to capture MMG sensor signals.

MMG sensor signal and motor control, the efficiency of patient movement will be improved by using LLRE.

2. Methods

2.1. Near-field electrospinning technology

Due to the PVDF piezoelectric properties of the MMG sensors, the dynamic signals of the patient motion intention can be captured precisely. The PVDF solution was prepared into uniform fibers with high piezoelectric properties by the near-field electrospinning technology as shown schematically in Fig. 1. During the fabrication from the solution to fibers, an external high-voltage electric field was applied between the injection needle and the roller collector. When the electrostatic force on the needle tip overcame the surface tension of the PVDF solution, a Taylor cone was formed at the tip of the needle and a fiber can be spun and collected. Due to the external high-voltage electric field, the fibers were polarized and orderly collected at the same time during the process.

For the electrospinning process, PVDF powder was prepared into two liquid solutions. The first solution consisted of acetone to dissolve PVDF powder (M.W. about 534,000 g/mole), and the second solution consisted of dimethyl sulfoxide with anionic fluorosurfactant. Anionic fluorosurfactant was used to reduce the surface tension of the PVDF solution, and to improve the wettability as well as the conductivity of PVDF solution during the NFES process. These advantages can increase the stability of the NFES process and the continuity of the production of piezoelectric fibers. Finally, two solutions were completed by mixing and stirring at a speed of 500 RPM for 60 min. The solution ratio is shown in supplementary materials.

2.2. Interdigitated electrode design

After the PVDF piezoelectric fibers were fabricated, the electrical signals induced by the piezoelectric fibers were collected through electrodes. To increase the signal-collecting efficiency, a planar interdigitated (IDT) electrode was introduced to collect the signals from the PVDF fibers. The electric charge accumulated on the PVDF fibers were effectively extracted when the fibers were deformed due to human body motion. In this experiment, ten groups of different interspaces and pairs of IDT electrodes were designed to examine the effects on the extraction voltage signals. The interspaces were designed as 0.2 mm, 0.4 mm, 0.6 mm, and the pairs in 1 pair, 5 pairs, 10 pairs and 15 pairs, respectively. Only 0.6 mm was designed for 1 pair and 5 pairs to avoid generating over-sized electrodes. The layout of the pairs and interspace are as schematically shown in Fig. 2. The material used in the IDT electrode was PAX-767-2, a halogen-free conductive silver paste supplied by Advanced Electronic Materials Inc. (ITK) with excellent electrical and physical properties. It has good fine line screen printing and adhere to PVDF fibers excellently. The material data of the IDT is shown in supplementary materials. For the production of electrodes, the screen printing and baking processes were adopted. The completed

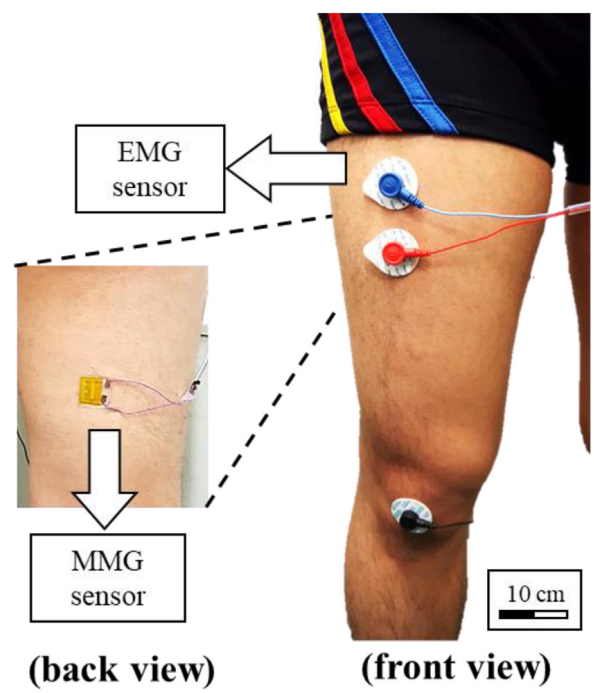

Fig. 4. Placement of MMG and EMG sensor in the human body.

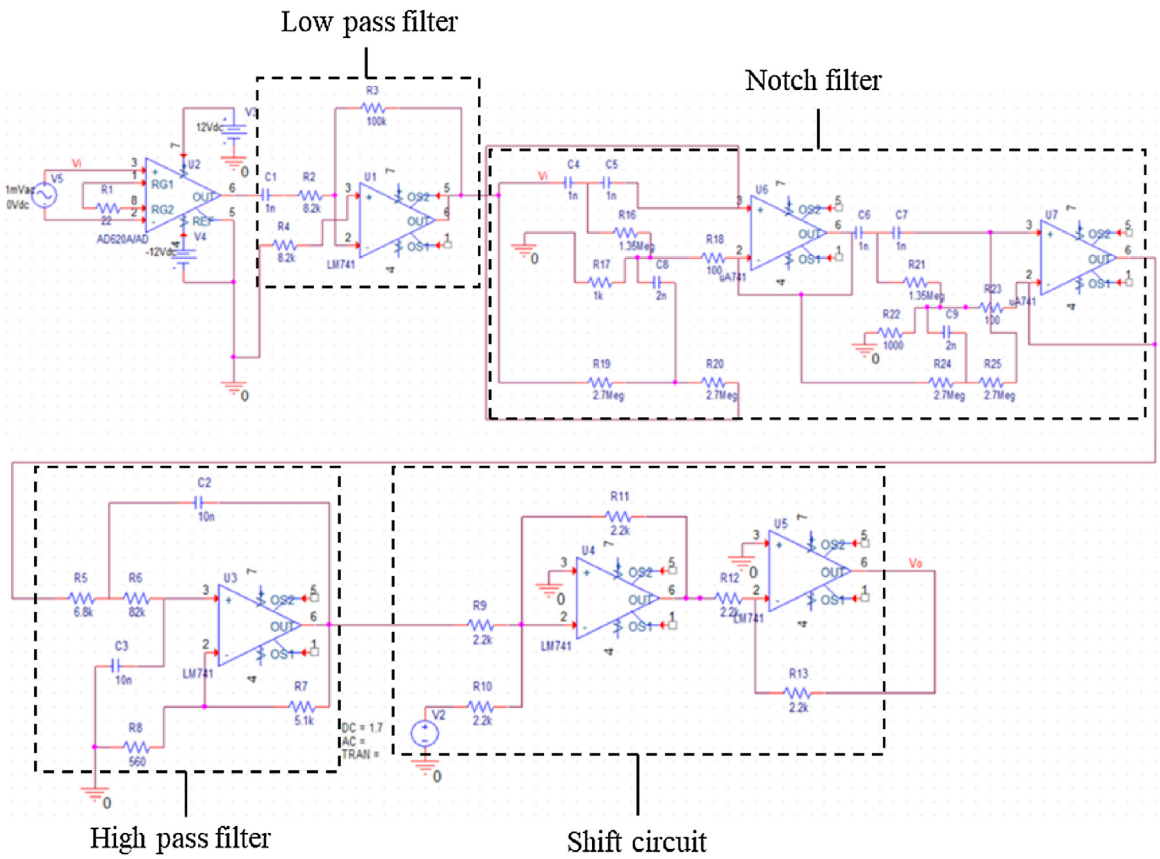

Fig. 5. Circuit for EMG/MMG signal process.

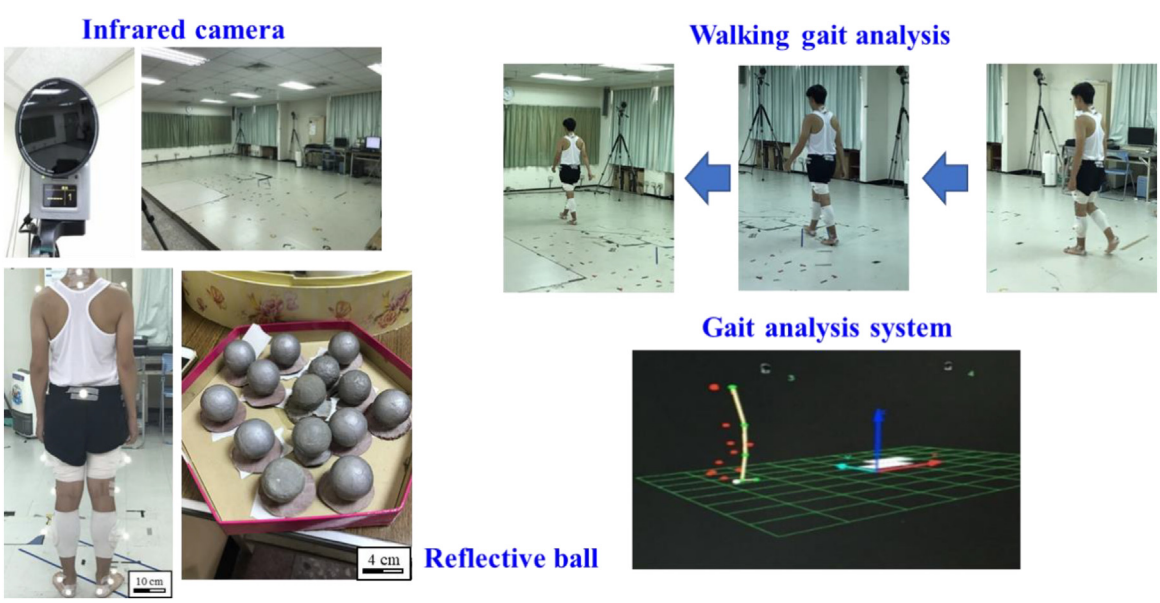

Fig. 6. Human gait measurement process.

fibers and IDT were packaged as MMG sensors and then tested as schematically shown in Fig. 3. Through the deformation of the fibers inside the MMG sensors, the signals due to piezoelectric effect was generated. For the electrical measurement, the voltage, current, and strain measuring instruments were used to determine which parametric combination showed the optimal electrical output.

2.3. Mechanomyography and electromyography signal processing

In order to examine which sensor is most appropriate for trigger LLRE during walking, a set of signal processing circuits was designed to identify the differences between the commercial EMG and the as-made MMG sensors. First, EMG signals were captured

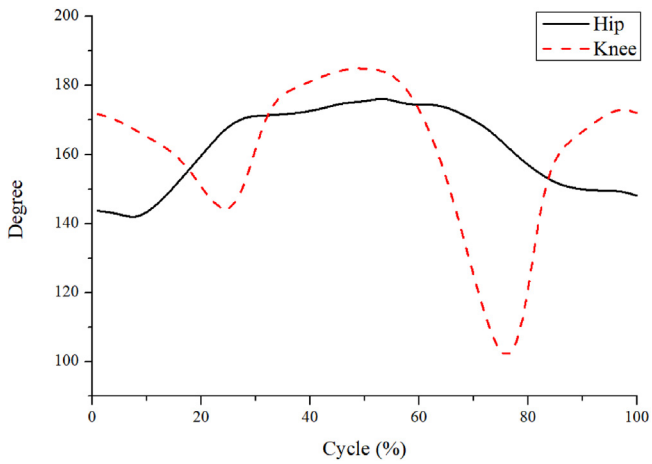

Fig. 7. The hip and knee joint angles over a gait cycle.

by bipolar, Ag–AgCl surface electrodes with a 2-cm interelectrode distance over rectus femoris. The ground electrode was attached to the skin over the patella. The MMG sensors developed in this study were attached to the biceps femoris, one of which forms part of the hamstrings muscle group, to capture the muscle deformation, as experimentally shown in Fig. 4. According to previous studies, the quadriceps muscle normally reaches its peak activation during the early stance phase in the gait cycle [24,25]. This characteristic can be used as reference to trigger LLRE. On the other hands, hamstring muscles activation begins in the late swing and peaks at heel-strike by an eccentric contraction, then rapidly contracts concentrically with knee flexion during initial heel strike [25,26]. As a result, huge deformations during lengthening/shortening (eccentric/concentric contraction) of activated muscle can be observed in the gait cycle. This feature can be used as trigger reference as well.

Because both EMG and MMG signals were very weak, signal amplification and analysis are required before entering the digital signal processor (DSP). The processing sequence was (1) the instrumentation amplifier, (2) the filter, and (3) the DSP. The AD620 was used in the instrumentation amplifier selection. It is a differential amplifier with a magnification of 10,000 times. However, due to the high magnification, a protection circuit was used to prevent electrostatic discharge at the input phase/stage.

The amplified signals were next filtered to eliminate the frequency band associated with the noise in the surrounding. First, a low-pass filter and a high-pass filter were set up to clean the unnecessary bands of frequency, especially in environmental electrical noise caused by the AC frequency at 50∼60 Hz. Then, a Notch filter was designed and used to address the concern. The overall filter circuit is shown in Fig. 5. Finally, the processed MMG/EMG signals were sent to the DSP, followed by the signal-to-noise ratio (SNR) analysis, as shown in Eq. (1), which was used to analyze this signal and serve as an on/off trigger switch of LLRE.

$$SNR = \frac{P_{signal}}{P_{noise}} = \frac{A^2_{signal}}{A^2_{noise}} \tag{1}$$

where P_{signal}, P_{noise}, A_{signal}, and A_{noise} are power of signal, power of noise, amplitude of signal and amplitude of noise, respectively.

2.4. Human gait measurement

The human gait data was measured by 6-camera Qualisys motion analysis system (Qualisys Inc., Gothenburg Sweden) to collect 3-dimensional coordinates of reflective markers placed bilaterally on bony landmarks of the participant's body: acromion process, greater trochanter, lateral epicondyle of the femur, lateral malleolus, heel, and lateral side of the thigh and shank, as shown in Fig. 6. The angle of knee and hip joints were calculated from 3-dimensional coordinate positions of the intended joint markers and two adjacent joint markers. Afterwards, these kinematic data of joint angles (in degrees) were reduced to 100 points representing equal intervals from 0% to 100% with respect to the gait cycle. The gait cycle was defined from heel strike to subsequent heel strike at the same limb. Gait events of the heel-strike and toe-off were identified by the vertical displacement of heel markers. For analysis purposes, the functional phases of gait were described by dividing the cycle into the stance and the swing phases, which usually occupy 60% and 40% of gait cycle at comfort speed respectively [27]. The hip and knee joint angles over a gait cycle were showed in Fig. 7. Afterwards, the gait data was stored in the master controller and then sent to the four-axis motor, which controlled hips and knees of both legs of LLRE.

2.5. Control system and mechanism of LLRE

The control system of LLRE is constructed as shown in schematically Fig. 8. The F28069 Piccolo and DRV8301 motor control board were used as the master and slave controller, respectively. F28069 Piccolo equipped with multiple sets of analog-to-digital converter (ADC) and digital-to-analog converter (DAC) channels, which was used to capture the signal from the EMG and MMG

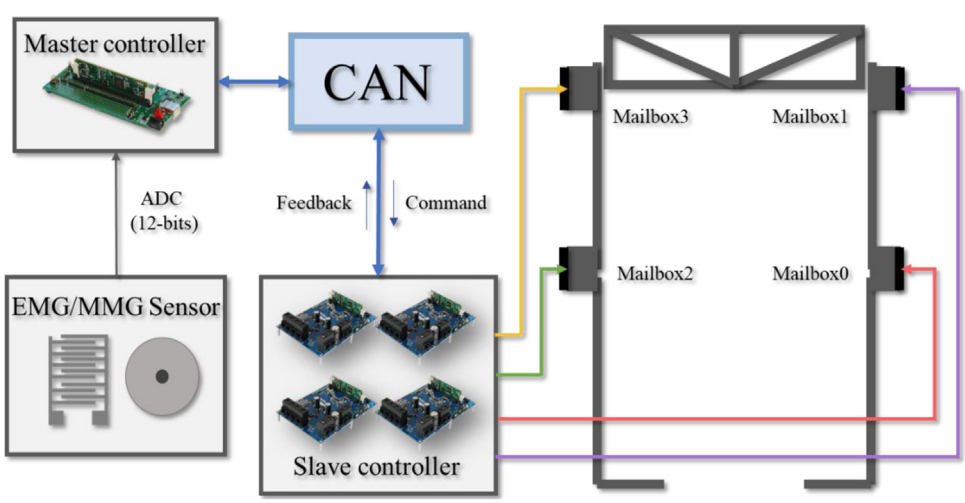

Fig. 8. Overall LLRE architecture with EMG/MMG sensors, master/slave motor controllers, and mechanisms.

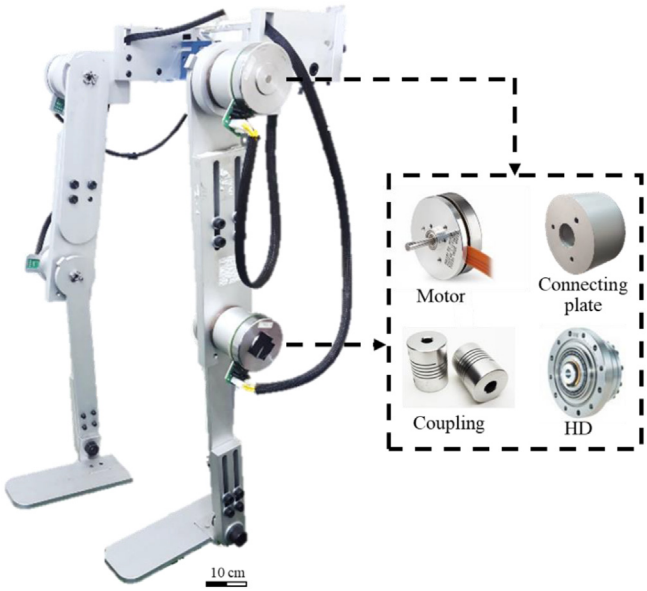

Fig. 9. Mechanism of the LLRE with 4 HDs and 4 slave motors.

sensors, respectively. The DRV8301 has multiple metal-oxide-semiconductor field-effect transistor (MOSFET) and was used to control the three phases of the motor. In order to accomplish the overall system, controller area network (CAN) was used as the communication interface between the master and slave controllers. The ADC of the master controller acquired the MMG and EMG sensor signals, signals were afterward analyzed, and the gait commands was sent to the slave controllers assigned.

The LLRE framework mechanism was designed to fit the lower limb structures of the human body and made it adjustable based on the height of the user, as shown in Fig. 9. There was a 1:100 harmonic drive (HD) between the motor and the mechanism, connected through the coupling. The effect of the HD greatly reduced the load of the joint torsion to increase the torque that the joint would withstand.

3. Results and discussion

3.1. Non-repolarized mechanomyography sensor

Fig. 10 shows the fabrication result of the packaged MMG sensors. First, the fibers obtained directly from the roller collector were examined by a SEM. The diameter of the electrospun PVDF fiber was about ~5-10 μm. Since the fibers were collected orderly, a compact fiber sheet was obtained. Then the fiber sheet was cut into a 40 mm × 8 mm in area and attached to a PET sheet printed with silver IDT electrodes. Finally, they were packaged together to complete the MMG sensor, as shown in Fig. 11.

To make a MMG sensor with better voltage signals output, the effect of different pairs and interspaces on the voltage was examined. A rotary signal tester was developed to beat the MMG sensor at a certain frequency. The experimental result of the voltage output is shown in Fig. 12. Regarding the effect of the interspace on the voltage signals, results reveal that the voltage increased as the interspace decreased. It was because when the interspace was smaller, the induced charges by the muscle deformation could be easier to reach the electrodes compared to those with larger interspaces. Regarding the pairs effect on the signal output, when the pairs were larger than 5, the voltages decreased gradually. More pairs indicate that the IDT consists of more effect of capacitors in parallel. Since the muscle deformation under the area covered by the sensors could be non-uniform, the average reading of the voltage signal might be unrepresentative. Therefore, the interspace and pair of the optimal combination were identified as 0.2 mm and 5, respectively, which has the largest voltage output.

Based on the result above, multiple sets of MMG sensors were made to measure the body motion signals. The voltage, current and strain signal output of a MMG sensor were measured and analyzed as shown in Fig. 13. The electrical measurement results of the IDT electrode with the pair and interspace were 5 and 0.2 mm. The MMG sensor has a significant voltage, current, and strain signal outputs of ~475 mV, 750 nA, and 400 $\mu\varepsilon$, respectively, at 9 Hz.

3.2. Repolarized mechanomyography sensor

To improve the MMG sensor signal output, the repolarization process was explored. In the re-polarization, the piezoelectric fibers were maintained under a high voltage of 750 V under tem-

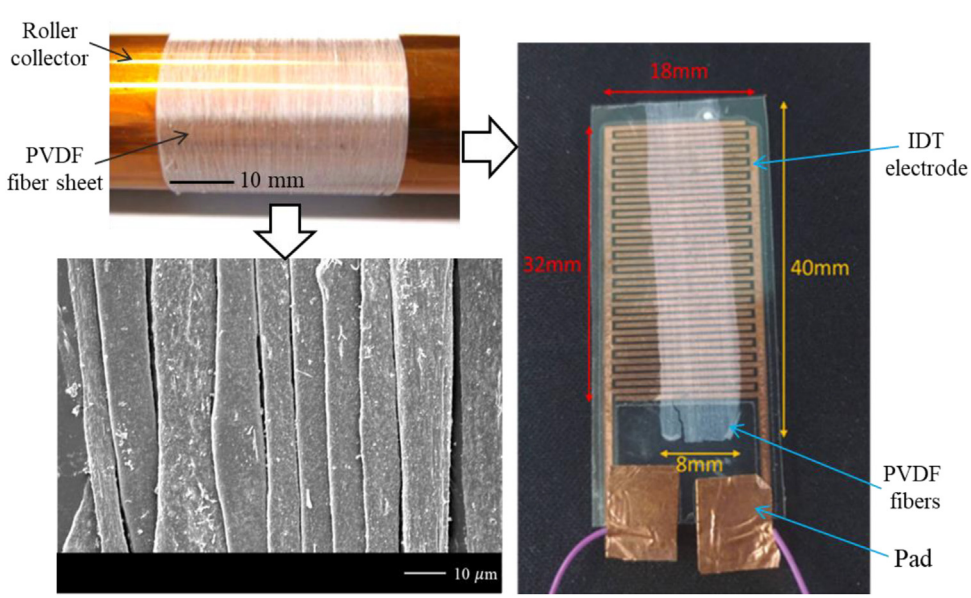

Fig. 10. The packaged MMG sensor.

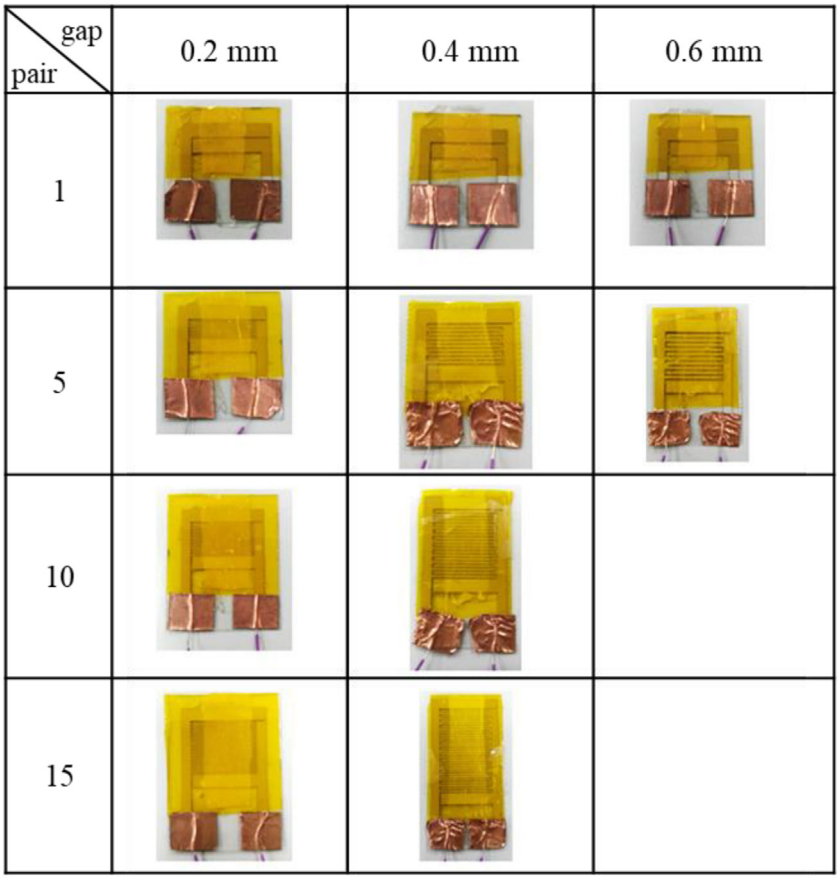

Fig. 11. MMG sensors with different pairs and interspaces.

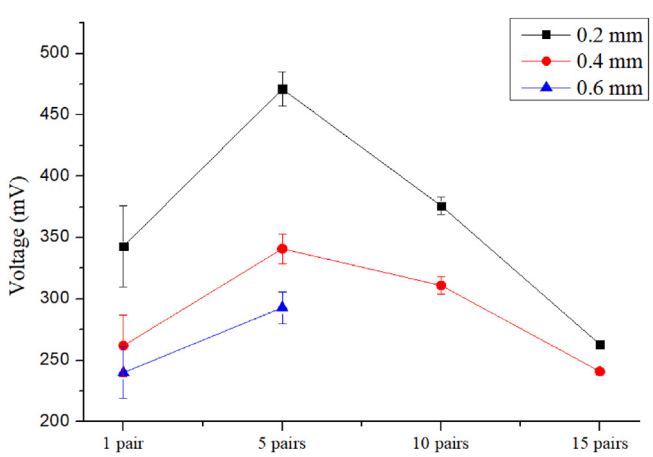

Fig. 12. Different combinations of IDT electrode voltage output.

perature 65° for 1 h. The repolarization occurred in the fiber length direction. After re-polarization, the piezoelectric fibers were divided into multiple groups, separated in terms of them of dipole moments. The dipole moment of the piezoelectric fibers was re-arranged in a more orderly manner to enhance the effect of charge addition. An illustration of the electric force lines for the sensors with the interdigital electrodes is shown in Fig. 14. The MMG sensor with a combination of 5-pairs and 0.2 mm interspace voltage generated the largest signal output about ~680 mV, as shown in Fig. 15. After the repolarization, the signals increased 43%. Therefore, this recipe was used later as the MMG sensor to measure human body motion. The strain signal represents the amount of deformation when the sensor was tested. The MMG sensor generates electrical properties through deformation rate, so the strain signal is used to prove the relationship of power generation.

Finally, to verify the stability of the MMG sensor, a fatigue test was performed, as shown in the Fig. 16. The result shows that under continuous 24 h of tapping, the output voltage had a very stable power generation and the waveform was not distorted.

3.3. Human body test using mechanomyography / electromyography sensors

Fig. 17 shows the layout of a filter circuit used for the MMG and EMG sensors. Due to the characteristic frequency band [28], the working range of MMG sensor was operated between ~20 Hz and 600 Hz, whereas the EMG sensor was operated between ~0.08 Hz and 300 Hz. First, the sensitivity and working frequency of MMG and EMG sensors were examined. A leg lifting up test with an EMG sensor is shown in Fig. 18(a). The EMG sensor signals generated a small signal during all movements as shown in Fig. 18(b) section S1 – S5. The maximum amplitude was about ~0.2 V and the SNR was about ~2.25, indicating that the EMG sensor is less sensitive during this slow movement test. Fig. 18(c) shows the test results of the MMG sensor. It is noted that there was a significant signal obtained even when the muscle vibrated and deformed at the same condition with the test of the EMG sensor. The maximum amplitude was about ~2.4 V and the SNR was about ~16. The largest MMG sensor signal was generated at the moment of the leg lifting up period (Fig. 18(c) section S2) due to the larger muscle deformation rate. Then, the trigger signal for LLRE was defined in section S2 of the MMG signal capture in a cycle. Compared to the MMG sensor,

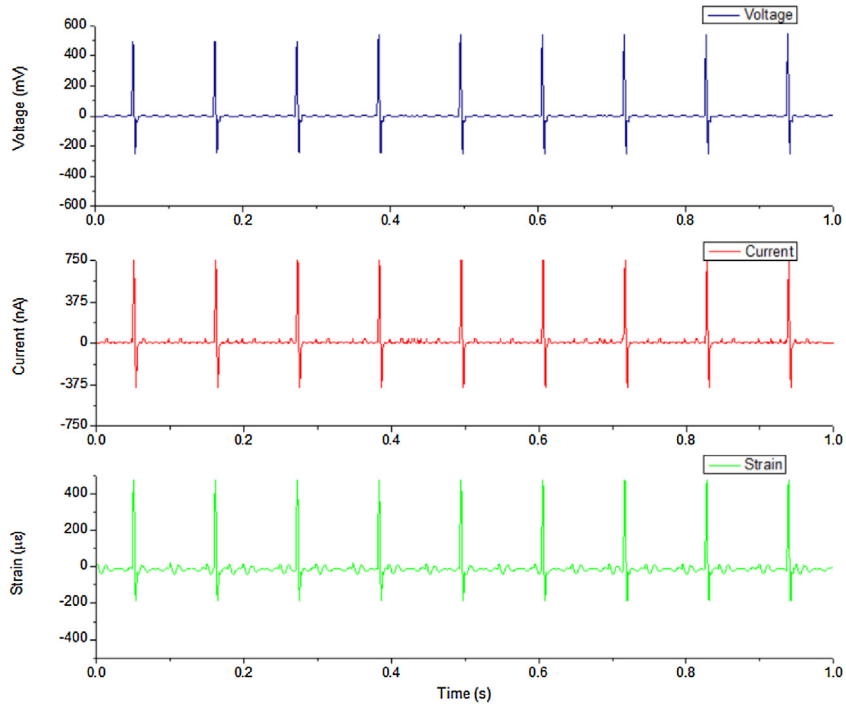

Fig. 13. The tapping test of the MMG sensors signal output at 9 Hz.

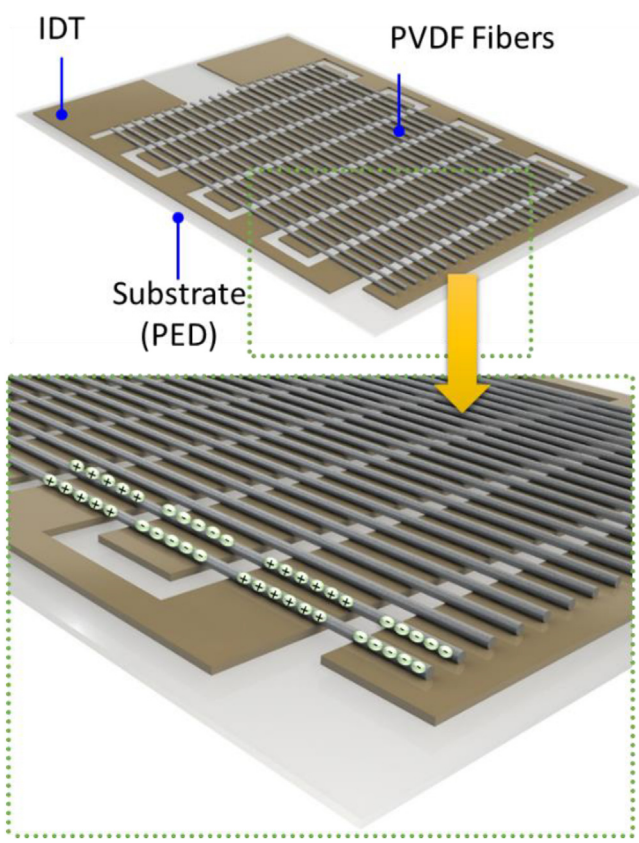

Fig. 14. Re-polarization of piezoelectric fibers on an IDT with a gap of approximately 0.2, 0.4 and 0.6 mm in pitch under a high voltage of 750 V for 1 h.

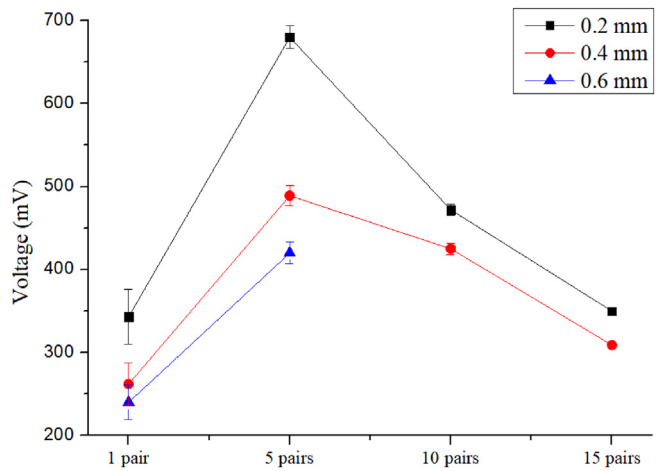

Fig. 15. Different combinations of IDT electrode and voltage output after repolarization.

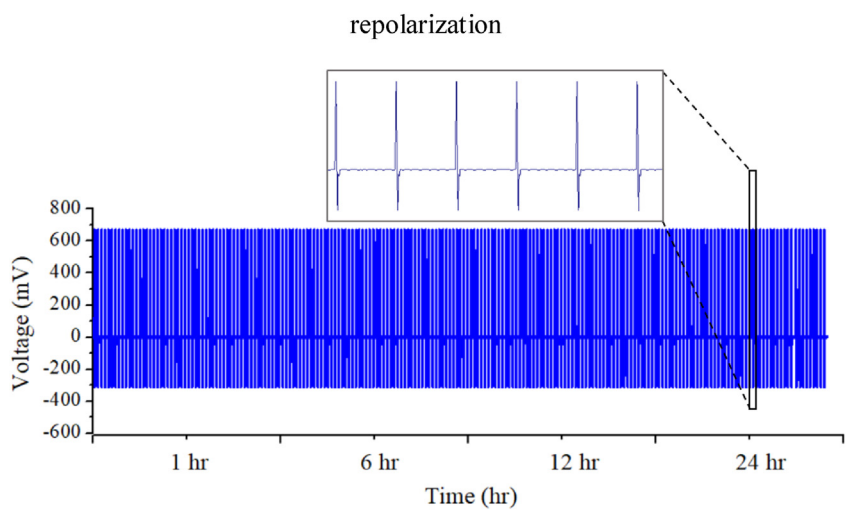

Fig. 16. Fatigue test of MMG sensor under continuous at the tapping of 9 Hz.

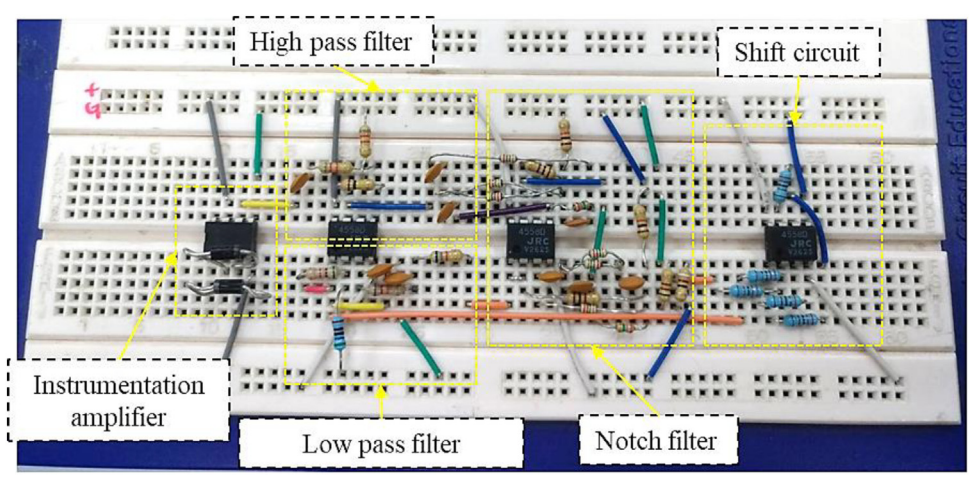

Fig. 17. Real connection diagram of MMG and EMG signal processing circuits.
(a) Sensors test of leg lifting up and lowering down
(b) EMG signal captured in a cycle
(c) MMG signal capture in a cycle

the EMG sensor required considerable motion of muscle to obtain obvious signals [28–30], and the signal was too small and unstable to function as triggers. Therefore, the MMG sensor was selected as an on/off trigger to actuate LLRE. Based on the experimentation, the MMG sensor developed in this study was sensitive enough to provide the DSP with an obvious intention on/off signal for the LLRE.

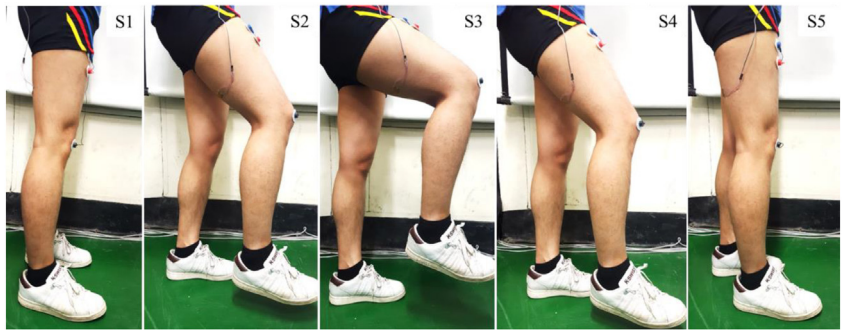

(a) Sensors test of leg lifting up and lowering down

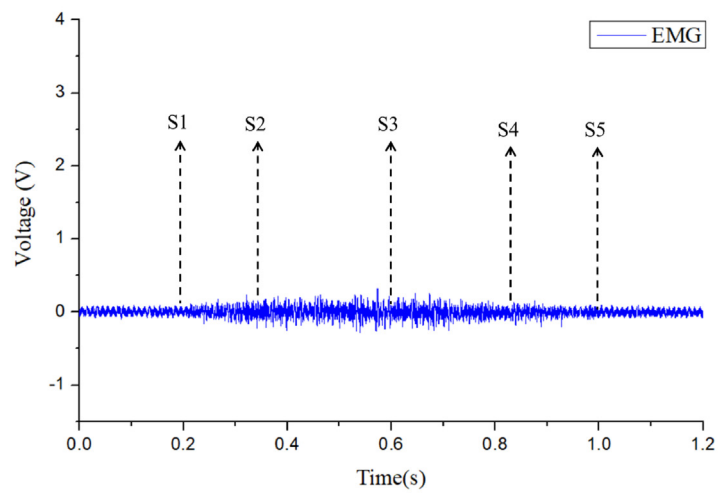

(b) EMG signal captured in a cycle

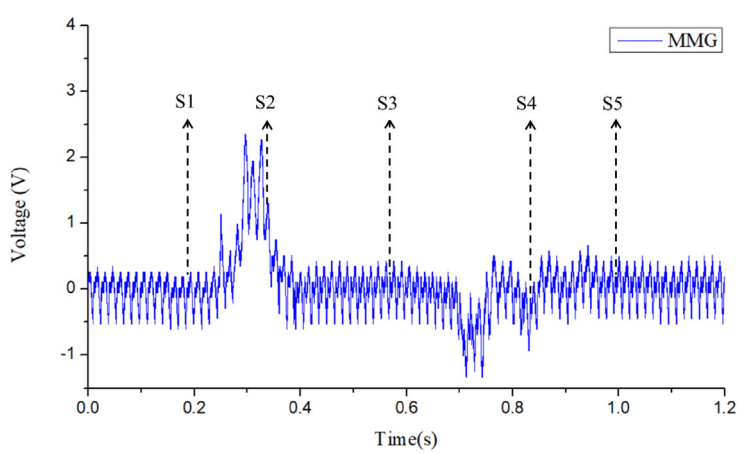

(c) MMG signal capture in a cycle

Fig. 18. Sensors signal captured in a cycle.

3.4. *Mechanomyography / electromyography* sensor test on LLRE system

Fig. 19 shows that the measurement of the EMG/MMG sensors' signals as on/off trigger switch of the LLRE in one human body. First, the EMG/MMG sensors' signals were captured and processed via an analog filter. Next, the signals were processed using the DSP program to determine the human motion intention. In the master controller, the signals were sampled at a fixed 2 kHz. Through the human walking gait data updated by signal activities, the system on/off signal triggered. The gait command was then transmitted through the CAN network from the master controller to the four slaves' controllers which were used to actuate the hips and knees of LLRE, respectively. Fig. 20 shows a human body wearing the LLRE. It is noted that the gait tracking of the knee and hip joints gave a good response.

Fig. 21 shows that during the walking process, the EMG sensor captured small amplitude of signals in the case of the muscle deformation activity. The maximum amplitude was about ~0.2 V and SNR was about ~4. On the other hand, the amplitude of the

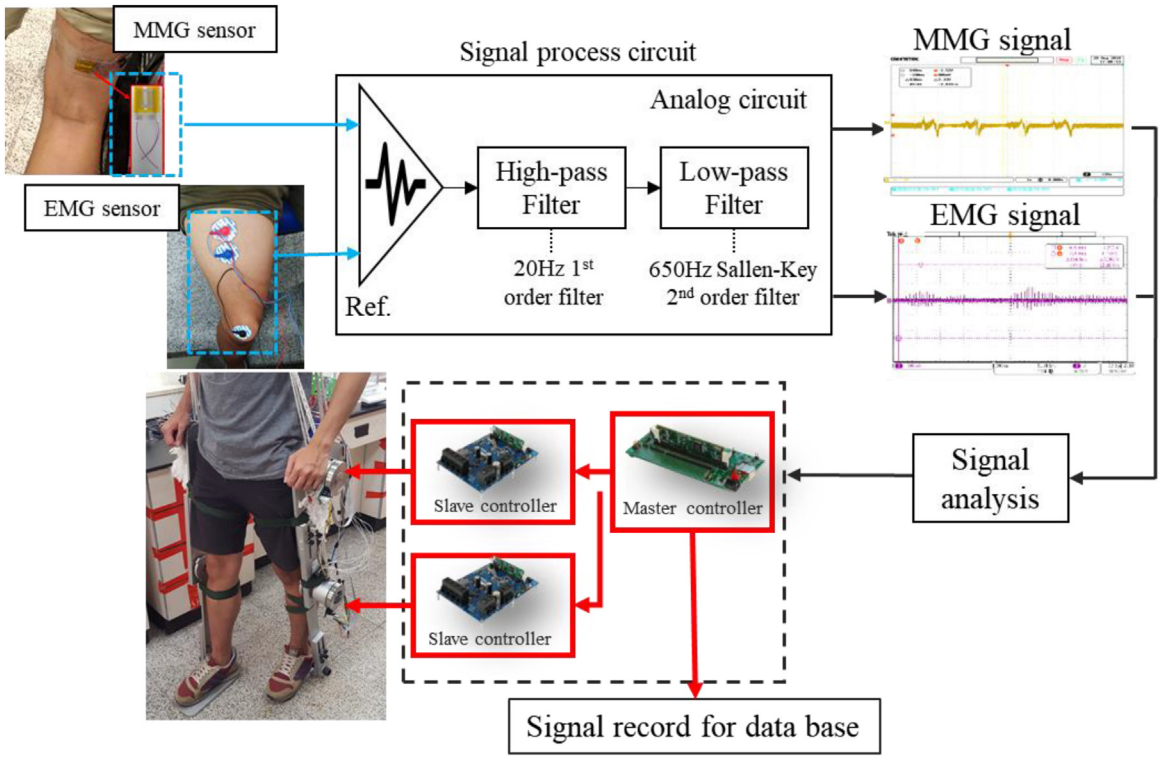

Fig. 19. The process of driving LLRE with MMG/EMG sensors' signals.

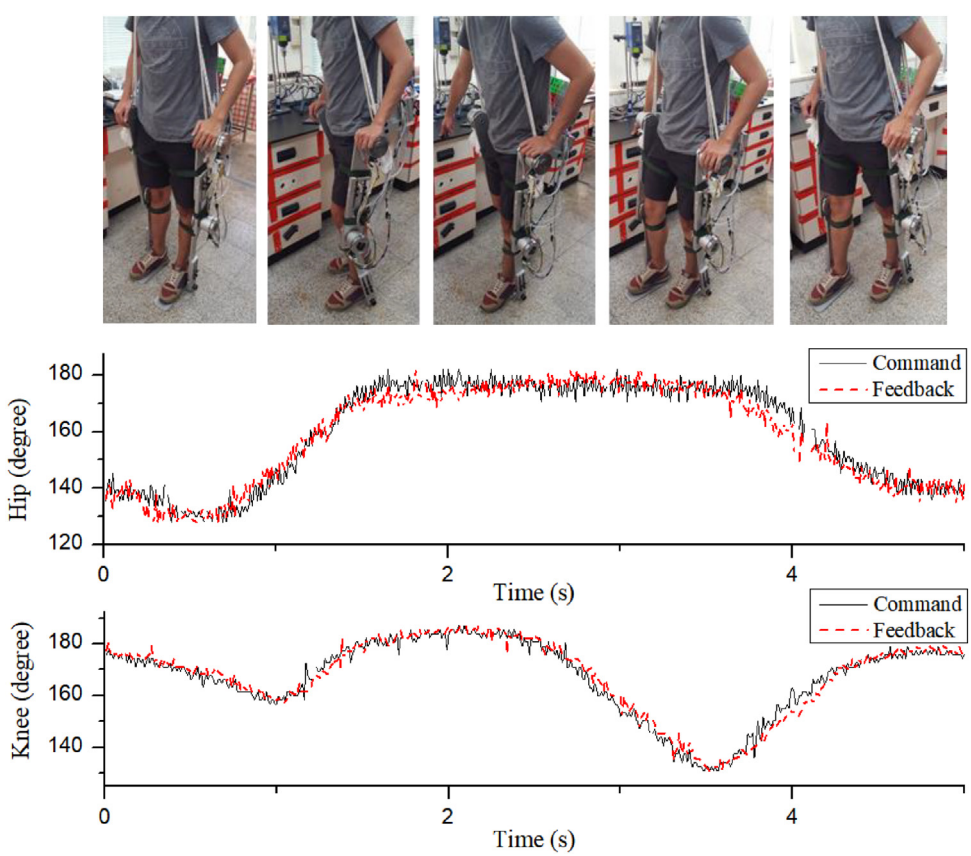

Fig. 20. The LLRE experiment in a gait cycle.

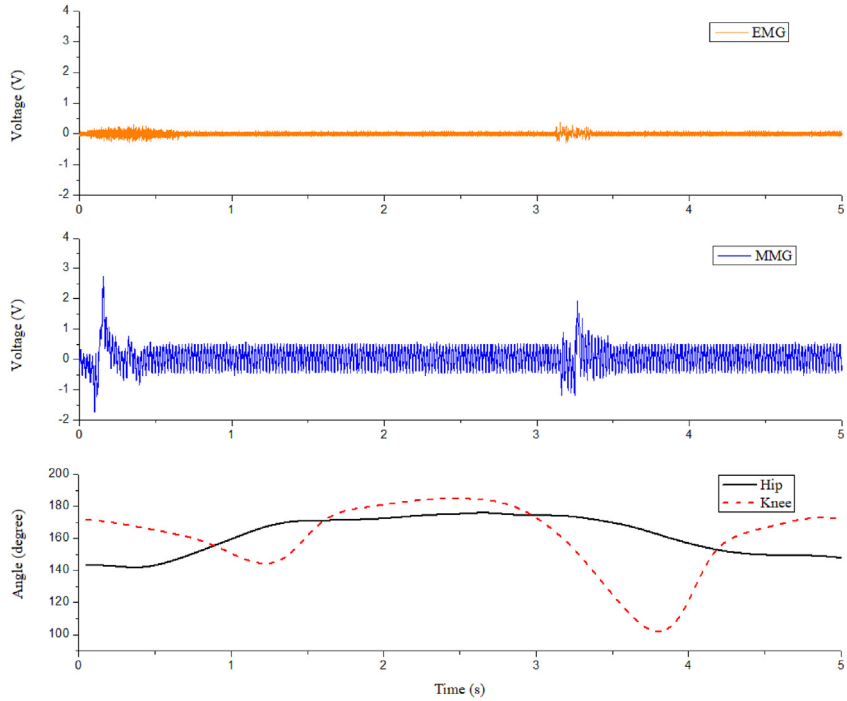

Fig. 21. Signal generated by EMG and MMG while walking.

MMG sensor signal was more recognizable than that of EMG. The moment of the leg lifting up signified the most obvious muscle activity. The maximum amplitude was about ~2.8 V and SNR was about ~25. Our results indicated that the MMG sensor could capture signals from muscle deformation and acted as a trigger on/off switch for the LLRE. Therefore, the MMG sensor could be utilized for physiological sensing applications.

4. Conclusions

In this study, a new type of fiber-based MMG sensor was developed and used as a motion on/off trigger sensor for LLRE. PVDF fibers attached on IDT electrode with different pole pairs and interspaces were packaged into an MMG sensor and electrical characteristics were tested. The results showed that the MMG sensor has a significant voltage output of ~475 mV at the rotary signal tester. After the repolarization, voltage generated the largest signal output about ~680 mV and the signals increased by 43%. Further, This MMG sensor was stuck on the thigh muscles to detect and acquire human motion intention signal, then trigger the controller and actuate the LLRE. The LLRE multi-axis control system included a master and four slave controllers to actuate the joints of hips and knees of both legs. The results showed that maximum signal amplitude and SNR of the MMG sensor were about ~2.8 V and ~25 and were 14 and 7 times compared to that of the EMG signals. In the fatigue test, the MMG sensor had good stability. During the LLRE walking process, the MMG sensor was successfully used for the on/off signal of the main controller to control the system of LLRE. Therefore, the developed MMG sensor has a higher sensitivity than commercial EMG sensor in driving the LLRE.

Declaration of Competing Interest

The authors declare that they have no known competing financial interests or personal relationships that could have appeared to influence the work reported in this paper.

Acknowledgments

The authors would like to thank the Ministry of Science and Technology, Taiwan for financially supporting this research under Contract no. MOST 106-2221-E-110 -032 -MY3.

Appendix A. Supplementary data

Supplementary material related to this article can be found, in the online version, at doi:https://doi.org/10.1016/j.sna.2019.111708.

References

[1] H.D. Lee, B.K. Lee, W.S. Kim, J.S. Han, K.S. Shin, C.S. Han, Human–Robotcooperation control based on a dynamic model of an upper limb exoskeleton for human power amplification, Mechatronics (2014) 168–176.
[2] M. Lowery, P. Nolany, Electromyogram median frequency, spectral compression and muscle fibre conduction velocity during sustained sub-maximalcontraction of the brachioradialis muscle, J. Electromyogr. Kinesiol. 12 (2002) 111–118.
[3] H. Kazerooni, R. Steger, The berkeley lower extremity exoskeleton, Trans. ASME, J. Dyn. Syst. Meas. Control 128 (March) (2006) 14–25.
[4] Y. Sankai, HAL: hybrid assistive limb based on cybernics, in: RoboticsResearch, Springer, 2011, pp. 25–34.
[5] C. Cescon, D. Farina, M. Gobbo, R. Merletti, R. Orizio, Effect of accelerometer location on mechanomyogram variables during voluntary, constant-force contractions in three human muscles, Med. Biol. Eng. Comput. (2004) 121–128.
[6] Keijiro Yamamoto, Stand alone wearable power assisting suit-sensing and control systems, Proceedings of the 2004 IEEE International Workshop on Robot and Human Interactive Communication (2004) 661–666.
[7] Gabi Zeilig, et al., Safety and tolerance of the ReWalk™ exoskeleton suit for ambulation by people with complete spinal cord injury: a pilot study, J. Spinal Cord Med. (2012), pp. 96-10.
[8] K. Kiguchi, Y. Imada, M. Liyanage, EMG-based neuro-fuzzy control of a 4DOF Upper-limb power-assist exoskeleton, 29th Annual International Conference of the IEEE/EMBS (2007) 3040–3043.
[9] R.A.R.C. Gopura, K. Kiguchi, Y. Li, SUEFUL-7: a 7DOF Upper-limb exoskeleton robot with muscle-model-oriented EMG-based control, IEEE/RSJ International Conference on Intelligent Robots and Systems (2009) 1126–1131.
[10] T. Lenzi, S.M.M.D. Rossi, N. Vitiello, M.C. Carrozza, Intention-based EMG control for powered exoskeletons, IEEE Trans. Biomed. Eng. 59 (8) (2012) 2180–2190.

[11] P. Madeleine, C. Cescon, D. Farina, Spatial and force dependency of mechanomyographic signal features, J. Neurosci. Methods 158 (2006) 89–99.
[12] M. Watanabe, K. Mita, K. Akataki, Y. Itoh, Mechanical behavior of condenser microphone in mechanomyography, Med. Biol. Eng. Comput. (2001).
[13] D.T. Barry, Acoustic signals from frog skeletal muscle, Biophys. J. 51 (1987) 5769–5773.
[14] K. Watanabe Mita, K. Akataki, K. Itoh, Reliability of the mechanomyogram detected with an accelerometer during voluntary contractions, Med. Biol. Eng. Comput. 41 (2003) 198–202.
[15] A. Kimoto, Y. Yamada, A new layered sensor for simultaneous measurement of EMG, MMG and oxygen consumption at the same position, Med. Biol. Eng. Comput. 53 (2015) 15–22.
[16] Akira Kimoto, Daisuke Aoki, A layered sensor for simultaneous measurement of skin water content and softness, Sens. Actuators A Phys. 217 (2014) 111–115.
[17] Akira Kimoto, I.E.E.E. Member, Shogo Shimada, A proposal of new multifunctional pressure sensor based on PVDF films, IEEE Trans. Instrum. Meas. 62 (10) (2013).
[18] Jipeng Yan, Xingchen Yang, Xueli Sun, Zhenfeng Chen, Honghai Liu, A lightweight ultrasound probe for wearable human–Machine interfaces, IEEE Sens. J. 19 (14) (2019).
[19] Kyle Van Volkinburg and Gregory Washington, Development of a wearable controller for gesture-recognition-based applications using polyvinylidene fluoride, IEEE Trans. Biomed. Circuits Syst. 11 (4) (2017).
[20] G. Gautschi, Piezoelectric sensorics: force, strain, pressure, acceleration and acoustic emission sensors, in: Materials and Amplifiers, Springer, 2002.
[21] C. Chang, K. Limkrailassiri, L. Lin, Continuous near-field electrospinning for large area deposition of orderly nanofiber patterns, Appl. Phys. Lett. (2008) 123.
[22] P. Sajkiewicz, A. Wasiak, Z. Goclowski, Phase transitions during stretching of poly (vinylidene fluoride), Eur. Polym. J. 35 (1999) 423–429.
[23] T.T. Wang, J.M. Herbert, A.M. Glass, The Applications of Ferroelectric Polymers, Br. Polym. J. 20 (1988) 533.
[24] M.O. Ericson, R. Nisell, J. Ekholm, Quantified electromyography of lower-limb muscles during level walking, Scand. J. Rehabil. Med. 18 (1986) 159–163.
[25] R. Shiavi, H.J. Bugle, T. Limbird, Electromyographic gait assessment, Part 1: Adult EMG profiles and walking speed, J. Rehabil Res. (1987) 13–23.
[26] B. Yu, R.M. Queen, A.N. Abbey, Y. Liu, C.T. Moorman, Garrett WE.Ḣamstring muscle kinematics and activation during overground sprinting, J. Biomech. 41 (2008) 3121–3126.
[27] J. Perry, Gait Analysis: Normal and Pathological Function, SLACK Incorporated, Thorofare, NJ, 1992.
[28] A. Kimoto, Y. Yamada, A new layered sensor for simultaneous measurement of EMG, MMG and oxygen consumption at the same position, Med. Biol. Eng. Comput. 53 (2015) 15–22.
[29] Nikos Karavas, Arash Ajoudani, Nikos Tsagarakis, Jody Saglia, Antonio Bicchi, Darwin Caldwell, Tele-impedance based assistive control for a compliant knee exoskeleton, Rob. Auton. Syst. 73 (November) (2015) 78–90.
[30] Hongchul Kim, Young June Shin, Jung Kim, Design and locomotion control of a hydraulic lower extremity exoskeleton for mobility augmentation, Mechatronics 46 (2017) 32–45.

Biographies

Dr. Cheng-Tang Pan is a Professor in the Department of Mechanical and Electro-Mechanical Engineering, NSYSU, Kaohsiung, Taiwan, and the Chair in the Institute of Medical Science and Technology, NSYSU, Kaohsiung, Taiwan. He is specialized in the field of medical assistive devices, motor control, nanofabrication, and LIGA process and the Co-Advising Professor of the primary author.

Chun-Chieh Chang was born in Kaohsiung, Taiwan, Republic of China, in 1993. He is studying in the Mechanical and Electro-Mechanical Engineering Department of Sun Yat-Sen University in Kaohsiung, Taiwan, Republic of China. His current research interests focus on electromechanical integration and motor controller design.

Dr. Yu-Sheng Yang graduated from the PhD program, School of Rehabilitation Science and Technology, University of Pittsburgh, USA, in 2005. He received his MA degree from Department of Occupational Therapy, New York University, USA, in 2000. Dr. Yang is currently an Associate Professor at the Department of Occupational Therapy, Kaohsiung Medical University, Kaohsiung, Taiwan. He also serves as Adjunct Occupational Therapist at Chung-Ho Memorial Hospital, Kaohsiung, Taiwan. The main research interests of Dr. Yang include assistive technology, wheelchair biomechanics, and motion analysis in human movement.

Dr. Chung-Kun Yen was born in Kaohsiung, Taiwan, 1980. He received his engineering degree of doctor in 2017, from Department of Mechanical and Electro-Mechanical Engineering of National Sun-Yat-Sen University in Kaohsiung, Taiwan. He current is post-doctor researcher in the Department of Mechanical and Electro-Mechanical Engineering of National Sun-Yat-Sen University in Kaohsiung, Taiwan. His current research interests focus on functional fibers, piezoelectric nanomaterials, flexible sensors, micro energy harvesting, lighting design, medical product design and universal design.

Yu-Hsuan Kao was born in Taoyuan, Taiwan, Republic of China. He is studying in the Mechanical and Electro-Mechanical Engineering Department of Sun Yat-Sen University in Kaohsiung, Taiwan, Republic of China. His current research interests focus on piezoelectric sensor and motor controller design.

Dr. Yow-Ling Shiue graduated from the PhD program, Animal Science and Genetics, University of California, Davis, USA. in 1996. Dr. **Shiue** is currently a Professor and Chair at the Institute of Biomedical Sciences, National Sun Yat-Sen University, Kaohsiung, Taiwan. His current research interests focus on genomics, gene regulation, bioinformatics and inducible stem cells/vaccines.